Input functions extraction from gated 18F-FDG PET images

CONFERENCE PAPER *in* IEEE NUCLEAR SCIENCE SYMPOSIUM CONFERENCE RECORD. NUCLEAR SCIENCE SYMPOSIUM · OCTOBER 2010

DOI: 10.1109/NSSMIC.2010.5874343

Input Functions Extraction from Gated ^{18}F-FDG PET Images

R. Mabrouk, L. Bentabet, F. Dubeau, M. Bentourkia

***ABSTRACT*--Derivation of the plasma time–activity curve in small animal positron emission tomography (PET) studies is a challenging task. Non-invasive input functions (IF) estimation in cardiac imaging usually involves drawing a region of interest (ROI) within the left ventricle (LV) of the heart. The small size of the LV relative to the resolution of the small-animal PET system, coupled with spillover and heart motion, makes this method difficult. In this work, we acquired rat cardiac images in list-mode with 16 ECG-gates with PET and ^{18}F-fluorodeoxyglucose (FDG). We introduced a customized coupled active contour model to reduce the image contamination from blood to tissue and from tissue to blood which are due to organ movements and spillover. The new findings were that we added an external energy to the internal contour to consider the contrast blood-to-tissue as important as the contrast tissue-to-outside myocardium. In order to correct the blood and tissue regions for spillover, we decomposed the two dynamic ROIs in their blood and tissue components using Bayesian probabilities. The results showed a good separation of the blood and tissue components in images as compared to the external blood sampling.**

I. Introduction

The Positron Emission Tomography (PET) imaging with ^{18}F-fluorodeoxyglucose (^{18}F-FDG) yields quantitative information on the biochemical processes of a radiopharmaceutical in a patient. The measurement of the radiotracer time course or time-activity curve (TAC) in both plasma (pTAC) and tissue (tTAC) is required to estimate the physiological parameters by means of pharmacokinetic models. The reference method to determine the plasma contents of the radiotracer delivered to tissue, or input function (IF), is an invasive blood sampling procedure to measure the tracer concentration in the arterial blood. This method was widely used to estimate IF for kinetic modeling and it is still used today in certain researches [1-3]. For small-animal ^{18}F-FDG PET studies, the blood sampling procedure is more difficult and challenging because of the small size of blood vessels and the limited blood volume, the time delay and dispersion in the tubing [4-5], effect of the noise [6-7], cross-calibration between samples and the PET scanner [8-10]. As an alternative approach, the population based input function is used for diverse studies in PET imaging. This technique requires previously collected data of blood sampling and these data are normalized with one or a few blood samples to obtain the IF for a specific measurement [11-16]. The IF can be obtained also directly from data by mean of region of interest (ROI) drawn on the blood pool in the case of cardiac imaging. In principle, this method is relatively simple to use. However, in small animal imaging, hearts and arteries are small compared to the scanner spatial resolution. Consequently, vascular radioactivity is blurred into adjacent tissues and vice versa. As a result, curves obtained from regions drawn over the vascular space are a mixture of the IF and the surrounding tissues. To avoid these problems, various methods have been proposed to estimate the IF noninvasively [17-21]. Some of these methods can be categorized as Factor Analysis for Dynamic Structures (FADS) and Independent Component Analysis (ICA)[22-25].The advantage of our method in comparison with ICA and FADS is that it does not need a dimension reduction of data, and does not need intermediate steps as oblique analysis for the FADS and cost function definition for ICA.

Manuscript received November 12, 2010

II. Materials and Methods

1. PET Measurements

Six Fischer rats of 200 ± 20 gr were injected with a bolus of 50 ± 5 MBq of ^{18}F-FDG and a 50 min dynamic list-mode acquisition was initiated. An iterative algorithm with Maximum Likelihood Expectation Maximization (MLEM) was used to reconstruct the images with 10 iterations in a grid of 160 x 160 voxels of size 0.5 x 0.5 x 1.175 mm. The rats were prepared and imaged while under anesthesia with isoflurane (1.5 % volume and 1 L/min oxygen flow) delivered through a nose cone. A venous catheter was installed into the caudal veins for the radioactive injection. A PE50 polyethylene catheter (Becton Dickinson) was inserted into the femoral artery for blood sampling. The preparation of the animals took around 20 minutes. During imaging, heart and respiration rates were monitored with and ECG and a respiration pillow (model 1025L SAII). The acquired data were reconstructed in 16 gates based on ECG timing where every gate is segmented on blood pool region and tissue region by means of active contours (AC). Also dynamic series of 26 frames were sorted out from the list-mode data, using the following sequence: 12 × 10 sec, 6 × 30 sec, 6 × 150 sec, 2 x 5 min and the remaining 20 min formed a separate image for a 3D volume viewing.

For partial volume correction, we used a phantom consisting in a Plexiglas cylinder of 75 mm diameter and having seven hollow cylinders of diameter 1, 3.4, 5.2, 8.7, 12.2, 14.2, 19.7 mm located at 28 mm from the phantom center. These hollow cylinders were filled with the same concentration of FDG and a single PET acquisition was obtained. The phantom scans were reconstructed in similar fashion as the rat scans. The hollow cylinders in the Plexiglas phantom image were used to determine the recovery coefficients (RC) for rat heart partial volume effect (PVE) correction.

The segmentation of the images with AC is processed on the gated images using the full data of the 30 min list-mode acquisition. Once the segmentation parameters are calculated, these are applied to the respective gates within each dynamic frame. We finally obtain blood and tissue TACs free from organ motion, spillover and PVE. These final TACs are used in kinetic modeling.

2. Active contours

Active contours were introduced by Kass *et al* [26] as a solution to boundary detection in a low-level imaging. A snake v is defined in the image plane (x,y) as a parametric curve of the curvilinear abscissae r at time t by: $v(r,t) = (x(r,t),y(r,t))$. The snake is allowed to deform from some arbitrary initial location within an image towards the desired final location. Thus, the use of snakes involves a two-step process: the initialization and the iterative minimization process. The final snake location is obtained through a minimization process acting upon the global energy (E_{tot}) of the snake defined as follows:

$$E_{tot}(t)=E_{int}(t)+E_{ext}(t) \quad (1)$$

where $E_{ext}(t)$ and $E_{int}(t)$ are the external and internal energies, respectively. The internal energy is introduced as:

$$E_{\text{int}}(t) = \oint (\alpha |v'(r,t)|^2 + \beta |v''(r,t)|^2) dr \quad (2)$$

where v', v'' are the first and second derivatives of the parametric curve respectively. The parameters α and β are Tikhonov stabilizers which control the elasticity (potential to stretch) and rigidity (potential to bend) of the snake.

In active contours framework, the external energy $(E_{ext}(t))$ is used to derive the external forces which acts on the snake to deform its shape and location. The relationship between external energy and forces is given by the following equation:

$$E_{ext}(t) = \oint |F_{ext}(v(r,t))| dr \quad (3)$$

Therefore internal force is associated with the shape of contour and external force is invoked by the edges or the lines of the object. In the rat PET image of the heart where we have to define heart cavity and heart tissue with two snakes, there is a significant difference between contrasts on image (Fig 1). Indeed, the interior boundary contrast of the myocardium muscle is lower than the exterior boundary. This difference is due to the contamination of the interior boundary by the blood pool.

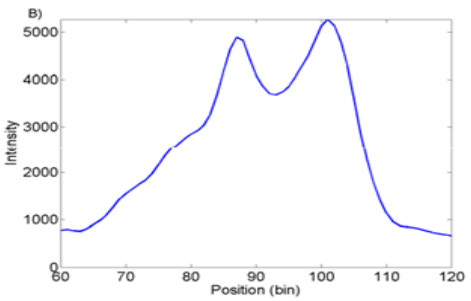

Fig.1. Projection activity: exterior boundary have a good contrast, the interior is fuzzy because of spatial resolution of detectors

In the proposed customized coupled snake model, two snakes are initialized on the same frame. An exterior snake detects the exterior boundary of the myocardium and an interior snake detects the interior boundary. If the external force used to simultaneously deform both snakes is defined using the classical gradient, the snakes could collide and converge to the same edge which is usually the exterior boundary of the myocardium. This fact results from the combination of two factors. Firstly, the gradient of the myocardium exterior boundary is stronger than the gradient of the interior boundary. Secondly, due to the small size of myocardium, the exterior and the interior snakes are initialized close to each other and hence they both could be attracted by the same strong edge.

To address this problem, an interaction term is introduced to avoid the collision of the two snakes. To achieves this goal, let's define a binary map $m(x,y,t)$ which provides the location of the exterior snake $v_{out}(r,t)$ at time t as follows:

$$m(x,y,t)=\begin{cases} 1 & If\ \exists r \in \Re \mid v_{out}(r,t)=(x,y) \\ 0 & otherwise \end{cases} \quad (4)$$

where (x,y) are the pixel's coordinates. The external energy of the interior snake is given by:

$$E_{ext}^{Inner}(t) = -\oint |\nabla I(v_{in}(r,t),t)| dr + \tau \times \oint |\nabla (G_\sigma (v_{out}(r,t) * m(v_{out}(r,t),t))| dr \quad (5)$$

where $v_{in}(r,t)$ is the interior snake and τ is a weighting parameter that controls the scale of the repulsive force. The external energy acting on the exterior snake is given by:

$$E_{ext}^{Outer}(t) = -\oint |\nabla I(v_{out}(r,t))| dr \quad (6)$$

Equations (5), and (6) show that the repulsive force is applied only on the interior snake.

3. Dynamic Parameters Setting

In order to track the myocardium motion, the snakes must shrink during the systolic phase and expand during the diastolic phase. The natural motion for a snake is shrinking which allows minimizing the total energy (1) by reducing the snake's length. The elasticity parameter α is usually set to some positive value, which results in the shrinking of the snake to minimize the quadratic form (2) used to define the internal energy. This is convenient for the systolic phase but not for the diastolic phase. During the diastolic phase, we propose to set α at some negative value for the interior snake. Consequently, the term $\oint (\alpha |v'(r,t)|^2 dr$ in (2) becomes negative. The minimization of the internal energy is possible only if the length of the snake increases, thus decreasing $\oint (\alpha |v'(r,t)|^2 dr$. Theoretically, without the action of $\oint \beta |v''(r,t)|^2 dr$ and the external energy, the expansion of the snake will continue forever and its total energy will tend to $-\infty$. To ensure a proper convergence to the desired edge, the total energy (1) must remain positive. Thus:

$$\oint (\alpha |v'(r,t)|^2 + \beta |v''(r,t)|^2) dr + E_{ext}^{Inner}(t) > 0 \quad (7)$$

As a result, α must satisfy the following:

$$-\frac{\beta\oint|v''(r,t)|^2 dr + E_{ext}^{Inner}(t)}{\oint|v'(r,t)|^2 dr} < \alpha < 0 \quad (8)$$

The condition above shows that it is possible to find a negative value for α which inflates the snake while keeping its total energy positive. To summarize, a positive α value is used during the systolic phase and a negative value is used during the diastolic phase for the interior snake.

4. Bayesian approach for spillover correction

When ROIs are drawn within the cavity of the left ventricle image obtained by the coupled contours, pTAC would equal the whole blood TAC. However, due to spillover and PVE, the model-predicted output of an image derived input function (IDIF) is expressed as a mixture of blood and tissue activity. This is also true for an ROI drawn around the tissue.

To resolve contamination of both regions, we use a simple and very efficient method namely the Bayesian approach. If we consider the concentration of the radiotracer in blood and tissue in time *t* as two classes $X_B(t)$ and $X_T(t)$, we can resolve cross-contamination by classification of pixel's activity. Let's denote a pixel belonging to blood ROI by:

$$X_B(s,t) = \begin{cases} \alpha_B(t)\cdot X(s,t) & \text{if} \quad X(s,t)\in BR \\ (1-\alpha_T(t))\cdot X(s,t) & \text{if} \quad X(s,t)\in TR \end{cases} \quad (9)$$

where *s* is the pixel index in the image, *X(s,t)* is the pixel value, $X_B(s,t)$ is the blood component, *BR* is the blood region, *TR* is the tissue region, $\alpha_B(t)$ is a fraction delimited in the interval [0 1] and refers to clean blood activity in blood ROI if its value is 1, and $\alpha_T(t)$ is tissue fraction. Similarly, a pixel belonging to tissue ROI is denoted by:

$$X_T(s,t) = \begin{cases} \alpha_T(t)\cdot X(s,t) & \text{if} \quad X(s,t)\in TR \\ (1-\alpha_B(t))\cdot X(s,t) & \text{if} \quad X(s,t)\in BR \end{cases} \quad (10)$$

where $X_T(s,t)$ is the tissue components in the tissue ROI. Given a set of data *X(s,t)*, the posterior probability of the fraction of $X_B(s,t)$ is defined as:

$$\alpha_B(t) = \frac{1}{n}\sum_n P(X_B(s,t)/X(t)) = \frac{1}{n}\sum_n \frac{P(X(s,t)/X_B(s,t))\times P(X_B(t))}{\sum_{i=\{B,T\}} P(X(t)/X_i(s,t))\times P(X_i(t))} \quad (11)$$

And given a set of data *X(s,t)*, the posterior probability of the fraction of $X_T(s,t)$ is defined as:

$$\alpha_T(t) = \frac{1}{n}\sum_n P(X_T(s,t)/X(t)) = \frac{1}{n}\sum_n \frac{P(X(s,t)/X_T(s,t))\times P(X_T(t))}{\sum_{i=\{B,T\}} P(X(t)/X_i(s,t))\times P(X(t))} \quad (12)$$

where $P(X(t)/X_B(s,t))$ is the likelihood of the model and $P(X_B(t))$ is the prior probability of the model. In Bayesian approach, evaluating the likelihood in (11) is often hard and much of the research in this area has focused on ways of doing it. A simple, but often reasonably good approximation of likelihood expression is defined as:

$$P(X(t)/X_B(s,t)) = \frac{n_B(X_B(t))}{N_B\times w_B} \quad (13)$$

where $n_B(X_B(t))$ is the intensity frequency on the blood ROI, N_B is the total number of pixels on region, and w_B is a sampling step of the intensity. The likelihood, as expressed in equation (13), acts as a weight for the prior probability at a given frame time *t*. he prior is inspired from the biological behavior of the radiotracer. Thus, after a bolus injection, the tracer diffuses into the tissue and consequently it is decreases with time. This temporal evolution can be modeled as an exponential distribution:

$$P(X_B(t)) = \lambda\times e^{-\lambda t} \quad (14)$$

where λ is a positive real number. This parameter is estimated from temporal data using Maximum Likelihood Estimator (MLE).

Similarly, for the tTAC estimation, the likelihood is defined as:

$$P(X(t)/X_T(s,t)) = \frac{n_T(X_T(t))}{N_T\times w_T} \quad (15)$$

where: $n_T(X_T(t))$, is an intensity frequency on the tissue ROI, N_T is the total number of pixels on tissue region and w_T is a sampling step of intensity.

As pointed previously, blood diffuses the ^{18}F-FDG radiotracer into the tissue which increases with time during the time of the PET measurement. Intuitively, we used as prior probability $P(X_T(t))$ the cumulative distribution function of a normal distribution.

$$P(X_T(t)) = \frac{1}{2}\times\left[1-erf\left(\frac{X_T(t)-\mu_{XT}}{2\times\sqrt{\sigma_{XT}}}\right)\right] \quad (16)$$

The parameters μ and σ of the normal distribution are estimated with MLE.

III. RESULTS AND DISCUSSION

The results of myocardium motion tracking are illustrated in Fig. 2 for the first and eighth gates. The results are satisfactory, and they show that the interior snake reaches its stability around the blood pool boundary and follows cardiac motion.

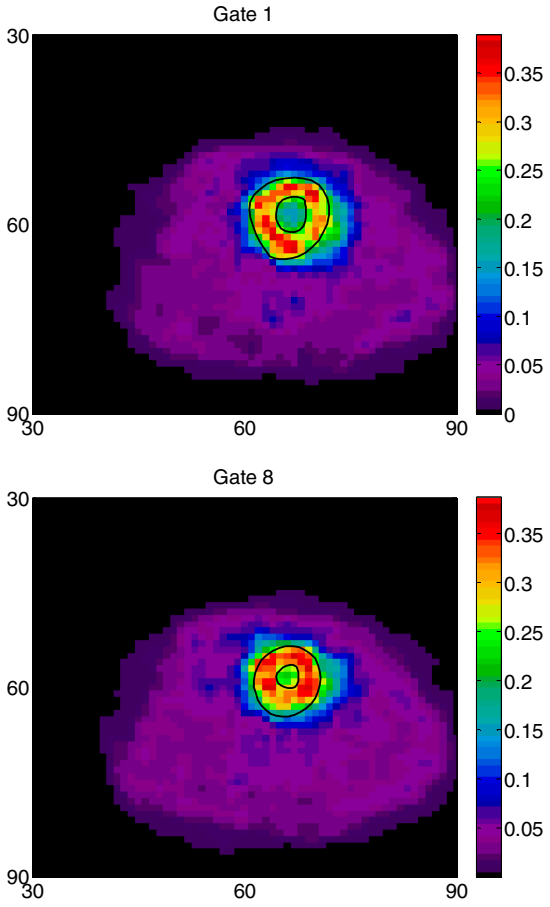

Fig.2: Gated images with ROIs automatically drawn with the new algorithm on gate 1 (above) and gate 8 (bottom).

Fig.3 displays a comparison between TACs obtained in the measured image and with AC followed with Bayesian signal separation. Fig. 3A shows the separation of the blood and tissue signals in the blood ROI, while Fig. 3B depicts signal separation in a tissue ROI, and both pairs of TACs are compared to the corresponding TAC obtained from the measured image. Fig. 3C presents a comparison between the calculated IF with AC and Bayes, the IF obtained from an ROI on the blood cavity and IF externally sampled. The differences between these IFs illustrate the effect of spillover in the IDIF and blood contamination and dispersion in the tubing of the sampled IF.

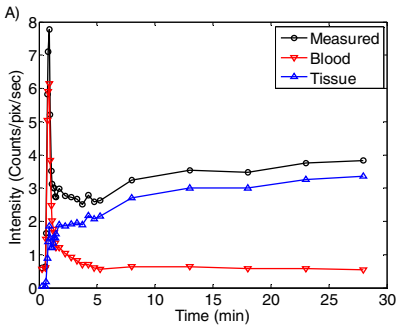

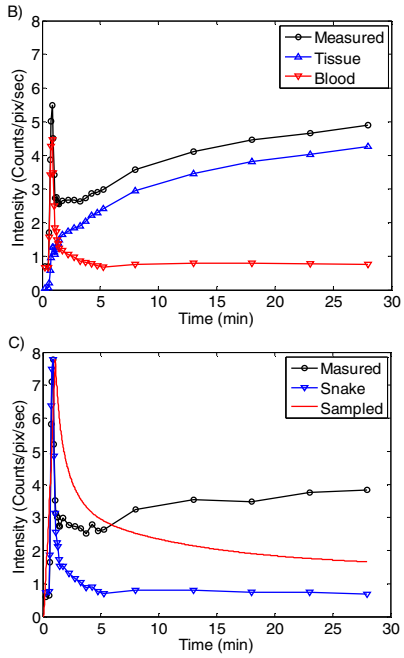

Fig. 3: Time-activity curves of blood and tissue in blood ROI (A) and in tissue ROI (B) in comparison to the same ROIs from the measured image (Measured). C) Comparison of IFs in the measured ROI (Measured), calculated with the new method (Snake) and with external samples (Sampled).

The calculation of myocardial metabolic rate of glucose (MMRG) values with IDIF and input function corrected by Bayes tools and corrected for the partial volume effect were both obtained in the tissue ROI from the measured image. This choice was made to compare the effects of the two input functions by applying them to the same tissue TAC. The usual statistical study (ANOVA) was applied to the six data analysis from the six rats and the results were reported as boxplots in Fig. 4.

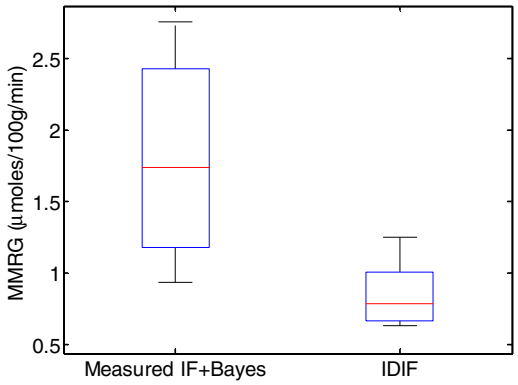

Fig. 4: Boxplot showing the variance between MMRG calculated with the usual (IDIF without correction) and MMRG calculated with Bayes IF for six Fischer rats.

The result depicted in Fig. 4 shows a difference between the MMRG value (0.8527± 0.2479 µmoles/100g/min) calculated with the usual (IDIF without correction) and MMRG value calculated with Bayes IF (1.8021± 0.7476 µmoles/100g/min). It is clear that the values calculated from the uncorrected

images are too low. This low value of uptake of the ^{18}F-FDG is related to the value of the input curve integral. Because of the IDIF contamination, its integral is high and consequently this involves a low value for MMRG. After correction of the input curve with AC, the Bayes tool and the correction for PVE, the calculated rate constants values appear more reliable and MMRG is comparable to the values found in the literature [27].

IV. CONCLUSION

We have presented a new method for extraction of time-activity curves from cardiac PET images in rats which inherently suffer from organ motions, partial volume effect and cross contamination between blood and tissue. The method is based on the addition of a gradient contour force to the common gradient image force in a customized active contour followed with a Bayesian approach to decompose image voxels in tissue and blood components. The modifications we made in the customized active contours allow us to minimize the contamination due to cardiac motion. The method was tested for segmenting blood pool and tissue using cardiac gated PET images of a small animal. A phantom and a Bayesian approach were used to correct respectively the partial volume effect and the cross-contamination of the blood by tissue and vice versa.

V. REFERENCE

[1] M. Bentourkia, A. Bol, A. Ivanoiu, C. Michel, A. Coppens, M. Sibomana , G. Cosnard, and D.E. Volder; standardized blood sampling scheme in quantitative FDG-PET studies. IEEE Transaction on Medical Imaging 1999; 18:379-384.

[2] B. Ronald, A. Van Linger, S. Van Balen, G. Hoving, and A. Lammertsa; Characteristics of a new fully programmable blood sampling device for monitoring blood radioactivity during PET. European Journal of Nuclear Medicine 2001; 28:81-89.

[3] L. Eriksson and I. Kanno; Blood sampling devices and measurements**.** Medical Progress through Technology 1991; 17:249-257.

[4] H. Iida, I. Kanno, S. Miura, M. Murakami, K. Takahashi, and K. Uemura; Error analysis of a quantitative cerebral blood flow measurement using H2 (15) O autoradiography and positron emission tomography, with respect to the dispersion of the input function. Journal of Cerebral Blood Flow Metabolism 1986; 6:536-545.

[5] J. Van den Hoff, W. Burchert, W. Muller-Schauenburg, G.J. Meyer, and H. Hundeshagen; Accurate local blood flow measurements with dynamic PET: Fast determination of input function delay and dispersion by multilinear minimization. Journal of Nuclear Medicine 1993; 34:1770-1777.

[6] R.H. Huesman; Equivalent methods to analyze dynamic experiments in which the input function is noisy. Physics in Medicine & Biology 1997; 42:147-153.

[7] K.W. Chen, C. Huang, and D Yu; The effects of measurement errors in the plasma radioactivity curve on parameter estimation in positron emission tomography. Physics in Medicine & Biology 1991; 36:1183-1200.

[8] V. Dhawan, J. Jarden, S. Strother, and A. Rottenberg; Effect of blood curve smearing on the accuracy of parameter estimates obtained for 82Rb/PET studies of blood-brain barrier permeability. Physics in Medicine & Biology 1988; 33:61-74.

[9] J. Kearfott; Performance of a well counter and a dose calibrator for quantitative positron emission tomography. Health Physics journal 1989; 57:623-629.

[10] D. Lapointe, J. Cadorette, S. Rodrigue, D. Rouleau, and R Lecomte; A microvolumetric blood counter/sampler for metabolic PET studies in small animals. IEEE Transaction in Nuclear Sciences 1998; 45:2195-2199.

[11] R. Boellaard, A. Van Lingen, S.C. Van Balen, B.G. Hoving, and A. Lammertsma. Characteristics of a new fully programmable blood sampling device for monitoring blood radioactivity during PET. European Journal of Nuclear Medicine 2001; 28:81-89.

[12] G.J. Cook, M.A. Lodge, P. Marsden, A. Dynes, and I. Fogelman; Non-invasive assessment of skeletal kinetics using fluorine-18 fluoride positron emission tomography: Evaluation of image and population-derived arterial input functions. European Journal of Nuclear Medicine 1999; 26:1424-1429.

[13] S. Takikawa, V. Dhawan, P. Spetsieris, W. Robeson, T. Chaly, R. Dahl, D. Margouleff, and D. Eidelberg; Noninvasive quantitative fluorodeoxyglucose PET studies with an estimated input function derived from a population-based arterial blood curve. Radiology 1993; 188:131-136.

[14] S. Eberl, A.R. Anayat, R. Fulton, P. Hooper, and M.J. Fulham; Evaluation of two population-based input functions for quantitative neurological FDG PET studies. European Journal Nuclear Medicine 1997; 24:299-304.

[15] J. Kissel, R. Port, J. Zaers, M. Bellemann, L. Strauss, U. Haberkorn, and G Brix; Noninvasive determination of the arterial input function of an anticancer drug from dynamic PET scans using the population approach. Medical Physics 1999; 26:609-615.

[16] K. Wakita, Y. Imahori, T. Ido, R. Fujii, H. Horii, M. Shimizu, S. Nakajima, K. Mineura, T. Nakamura, and T. Kanatsuna; Simplification for measuring input function of FDG PET: Investigation of 1-point blood sampling method. Journal of Nuclear Medicine 2000; 41:1484-1490.

[17] Y.H. Fang, T. Kao1, R.S. Liu, and L.C. Wu; Estimating the input function non-invasively for FDG-PET quantification with multiple linear regression analysis: simulation and verification with in vivo data. European Journal of Nuclear Medicine 2004 31; 692-702.

[18] S.C. Huang, M.E. Phelps, E.J. Hoffman, K. Sideris, C.J. Selin, and D.E. Kuhl; Noninvasive determination of local cerebral metabolic rate of glucose in man. American Journal of Physiology 1980; 238:69-82.

[19] K. Chen *et al*; Noninvasive quantification of the cerebral metabolic rate for glucose using positron emission tomography, 18F-fluoro-2-deoxyglucose, the Patlak method, and an image-derived input function. Journal of Cerebral Blood Flow & Metabolism 1998; 18:716-723.

[20] T. Ohtake *et al*; Noninvasive method to obtain input function for measuring tissue glucose utilization of thoracic and abdominal organs. Journal of Nuclear Medicine 1991; 32:1432-1438.

[21] L.A. Green, *et al*; Noninvasive methods for quantitating blood time-activity curves from mouse PET images obtained with fluorine-18-fluorodeoxyglucose. Journal of Nuclear Medicine 1998; 39:729-734.

[22] A. Sitek, E.V.R. Di Bella, and G.T. Gullberg; Factor analysis with a priori knowledge - application in dynamic cardiac SPECT. Physics in Medicine & Biology, 2000 45:2619-2638.

[23] H.M. Wu, C.K. Hoh, Y. Choi, H.R. Schelbert, R.A Hawkins, M.E. Phelps, and S.C. Huang ; Factor Analysis for Extraction of Blood Time-Activity Curves in Dynamic FDG-PET Studies. Journal of Nuclear Medicine 1995; 36:1714-1722.

[24] M. Naganawa, Y. Kimmura, K. Oda, K. Ishiwata, and A.Matani; Extraction of a plasma time-activity curve from brain PET images based on independent component analysis. IEEE Transaction on Biomedical Engineering 2005; 52:201-210.

[25] M. Naganawa *et al*; Omission of serial arterial blood sampling for quantitative analysis of monkey PET data using independent component analysis-based method. ieee NSS/MIC 2007.

[26] Kass M, Terzopoulos D. Snakes: active contour models Int J of Computer Vision 1988;1: 321:331 .

[27] Lahcen Arhjoul and M'hamed Bentourkia; Assessment of glucose metabolism from the projections using the wavelet technique in small animal pet imaging, Comput Med Imag Graph 2007; 31:157:165